Antiferromagnetic spin structure and lithium ion diffusion in Li_2MnO_3 probed by μ^+SR

Jun Sugiyama,[1,*] Kazuhiko Mukai,[1] Hiroshi Nozaki,[1] Masashi Harada,[1] Martin Månsson,[2] Kazuya Kamazawa,[3] Daniel Andreica,[4] Alex Amato,[5] and Adrian D. Hillier[6]

[1]*Toyota Central Research and Development Laboratories, Inc., Nagakute, Aichi 480-1192, Japan*
[2]*Laboratory for Solid State Physics, ETH Zürich, CH-8093 Zürich, Switzerland*
[3]*Comprehensive Research Organization for Science and Society, Tokai, Ibaragi 319-1106, Japan*
[4]*Faculty of Physics, Babes-Bolyai University, 3400 Cluj-Napoca, Romania*
[5]*Laboratory for Muon Spin Spectroscopy, Paul Scherrer Institut, CH-5232 Villigen PSI, Switzerland*
[6]*ISIS Muon Facility, Rutherford Appleton Laboratory, Didcot, Oxfordshire, OX11 0QX, United Kingdom*

(Received 23 August 2012; revised manuscript received 17 October 2012; published 14 January 2013)

In order to elucidate the antiferromagnetic (AF) spin structure below $T_N \sim 35$ K and to clarify the diffusive behavior of Li^+ ions in the layered compound Li_2MnO_3, we have performed a muon-spin rotation and relaxation (μ^+SR) experiment using a powder sample in the temperature range between 2 and 500 K. Below T_N, the zero-field (ZF-) μ^+SR spectrum showed a clear oscillation that consists of two muon-spin precession signals with different frequencies. Combining with the dipole field calculations, it was found that the most probable spin structure for Li_2MnO_3 is the C_x-type AF order in which Mn moments align parallel or antiparallel to the a axis in the $[Li_{1/3}Mn_{2/3}]O_2$ layer, and a ferromagnetic chain along the a axis aligns antiferromagnetically along both the b and c axes. The ordered Mn moment was estimated as $2.62\mu_B$ at 2 K. In the paramagnetic state, ZF- and longitudinal-field μ^+SR spectra exhibited a dynamic nuclear field relaxation. From the temperature dependence of the field distribution width, the Li^+ ions were found to diffuse mainly along the c axis through the Li ion in the $[Li_{1/3}Mn_{2/3}]O_2$ layer. Also, based on the field fluctuation rate, a self-diffusion coefficient of Li^+ ions (D_{Li}) at 300 K was estimated as $4.7(4) \times 10^{-11}$ cm^2/s with the thermal activation energy $E_a = 0.156(3)$ eV.

DOI: 10.1103/PhysRevB.87.024409 PACS number(s): 76.75.+i, 75.25.−j, 75.50.Ee, 66.30.H−

I. INTRODUCTION

Alkali transition-metal dioxides, AMO_2, with an α-$NaFeO_2$-type structure were originally studied due to their complex magnetic nature caused by a competition between geometrical frustration and antiferromagnetic (AF) correlation on the two-dimensional triangular lattice of M ions,[1–3] which is formed by a network of edge sharing MO_6 octahedra. Besides the strong interests in their magnetism from the viewpoint of condensed matter physics, AMO_2, particularly $LiMO_2$, has been heavily investigated as a positive electrode material for Li-ion batteries due to a reversible extraction (insertion) reaction of Li^+ ions from (into) the lattice.[4–7]

The target compound, Li_2MnO_3, belongs to a monoclinic system with $C2/m$ space group, and $a = 0.4937$ nm, $b = 0.8532$ nm, $c = 0.5032$ nm, and $\beta = 109.46^\circ$ at ambient temperature (T)[8] (see Fig. 1). Since the Li_2MnO_3 structure consists of alternating stack of a Li plane and $[Li_{1/3}Mn_{2/3}]O_2$ layer along the c axis, Li_2MnO_3 could be also classified as a layered AMO_2.

Magnetically, Li_2MnO_3 is known to be an AF insulator with $T_N \sim 50$ K.[9,10] Neutron diffraction measurements[8] revealed that the AF unit cell is doubled along the c axis. In addition, the AF spin structure was proposed as an A-type AF order, in which the Mn moments align ferromagnetically along the c axis in the $[Li_{1/3}Mn_{2/3}]O_2$ layer, but antiferromagnetically between the adjacent $[Li_{1/3}Mn_{2/3}]O_2$ layers. However, since another structure was also proposed in Ref. 8, the AF spin structure is still not fully understood at present.

Electrochemically, Li_2MnO_3 was found to exhibit a reversible extraction-insertion reaction of Li^+,[11] which led to an intensified effort to clarify the relationship between structural and/or physical parameters and electrochemical properties.[12–18] Detailed electrochemical measurements combined with XRD analysis suggested the formation of oxygen deficiency during extraction-insertion reactions in order to keep charge neutrality.[19,20] This was supported by recent first-principles calculations.[21] As a result, the Li_2MnO_3 phase gradually transforms into a spinel-like phase during the extraction reaction.[22] Furthermore, since a solid solution system between Li_2MnO_3 and $LiMO_2$ has a very high capacity compared with those of the conventional positive electrode materials,[19] such "Li_2MnO_3-stabilized $LiMO_2$" compounds are extensively investigated as a positive electrode material for the future Li-ion batteries.[23]

Despite a main stream of research towards the battery application, the nature of Li_2MnO_3, particularly, a correct AF spin structure and a diffusive behavior of Li^+ ions, are still not clarified so far. If the A-type AF order is formed below T_N, as in the case for $NaNiO_2$,[24] the interaction between the neighboring Mn ions is naturally ferromagnetic (FM), and the interaction via an Mn-O-Li-O-Mn path is AF along the c axis. However, such interaction should be FM or negligibly small in the $[Li_{1/3}Mn_{2/3}]O_2$ layer. In order to further elucidate the magnetic nature of Li_2MnO_3, we have made a positive muon-spin rotation and relaxation (μ^+SR) experiment, because μ^+SR provide information on magnetic environment at the vicinity of implanted muons. Indeed, μ^+SR clarified the magnetic nature of many AMO_2 compounds, such as $LiCrO_2$,[25,26] $NaCrO_2$,[27] Li_xCoO_2,[28,29] Na_xCoO_2,[30–35] K_xCoO_2,[36,37] Li_xNiO_2,[38,39] and $NaNiO_2$.[40] Although preliminary results on Li_2MnO_3 were already described elsewhere,[41,42] we definitely need more detailed analysis in order to determine the AF spin structure.

Concerning Li diffusion, since magnetic ions in the lattice strongly affect a Li-NMR signal even in a paramagnetic

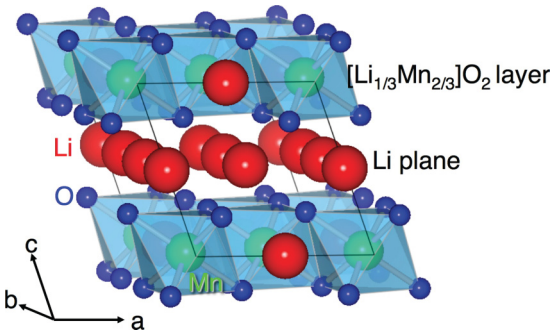

FIG. 1. (Color online) Crystal structure of Li_2MnO_3. Solid lines represent a crystallographic unit cell.

state of Li_xCoO_2,[43,44] it is extremely difficult to measure a spin-lattice relaxation rate ($1/T_1$) caused by Li diffusion. In fact, past Li-NMR work on Li_2MnO_3 did not yield a self-diffusion coefficient of Li^+ (D_{Li}).[45,46] Furthermore, due to a structural transformation during the Li^+ extraction reaction and a lack of information on the correct surface area between electrode and electrolyte, it is difficult to estimate D_{Li} for Li_2MnO_3 by electrochemical measurements. Hence, although D_{Li} is one of the most fundamental parameters to explain the rate of the extraction-insertion reaction, both Li-NMR and electrochemical measurements provide a very rough estimate for D_{Li}.

On the contrary, μ^+SR is found to give more reliable D_{Li} in Li_xCoO_2[47] than Li-NMR,[44] where Li_xCoO_2 is known to be a common cathode material for Li-ion batteries,[4] This is because muons do not feel fluctuating magnetic moments at high T, but instead sense the change in nuclear dipole field due to Li diffusion. Even if magnetic moments still affect the muon-spin depolarization rate, such an effect is, in principle, distinguishable from that of nuclear dipole fields.[48] In particular, a weak longitudinal field (LF) can be applied that decouples the magnetic and nuclear dipole interactions.[49] Here, LF means the magnetic field parallel to the initial muon-spin polarization. Following upon the initial attempt for measuring D_{Li} by μ^+SR,[47] the diffusive nature has been investigated for $LiNiO_2$,[39] $LiCrO_2$,[39] $Li_x(Co_{1/3}Ni_{1/3}Mn_{1/3})O_2$,[50] and $LiMPO_4$ with M = Fe, Co, Ni.[51–53] Here, we report the μ^+SR results of Li_2MnO_3 in order to clarify both the AF ground state at low T and the diffusion path and D_{Li} at high T.

II. EXPERIMENTAL

A powder sample of Li_2MnO_3 was prepared by a solid-state reaction technique between $LiOH{\cdot}H_2O$ and MnOOH (Li/Mn = 2.00/1.00) at 900 °C under air for 12 h. According to a powder x-ray diffraction (XRD) analysis, the sample was assigned as a single phase of a monoclinic symmetry with space group $C2/m$.

In order to know the macroscopic magnetic properties of the sample, susceptibility (χ) was measured below 400 K under a $H \leqslant 10$ kOe field with a superconducting quantum interference device (SQUID) magnetometer (MPMS, Quantum Design). The Weiss temperature (Θ_{CW}) and effective magnetic moment (μ_{eff}) were determined from the $\chi(T)$ curve by fitting to a Curie-Weiss law, $\chi = C/(T - \Theta_{CW})$ and

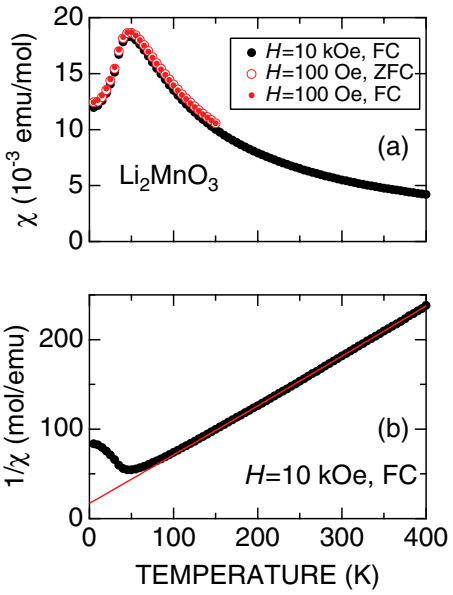

FIG. 2. (Color online) T dependence of (a) susceptibility (χ) and (b) $1/\chi$ for Li_2MnO_3. The χ data were obtained in field cooling (FC) mode with $H = 10$ kOe. In (a), the data obtained in FC and zero-field cooling (ZFC) mode with $H = 100$ Oe are also plotted for comparison. In (b), the solid line represents a linear fit in the T range between 200 and 400 K using a Curie-Weiss formula.

$C = (N/3k_B)\mu_{eff}^2$ in the T range between 200 and 400 K. Here, N is the density of Mn spins, μ_{eff} is the effective magnetic moment per Mn, and k_B is Boltzmann's constant. As a result, we obtained $\Theta_{CW} = -32 \pm 2$ K and $\mu_{eff} = 3.86 \pm 0.02\mu_B$, respectively (see Fig. 2). These values are similar to those for polycrystalline samples found in the literature.[9,10]

The μ^+SR spectra were measured at the surface muon beam lines using the Dolly spectrometer of SμS/PSI in Switzerland and the MuSR spectrometer of ISIS/RAL in United Kingdom. At PSI, the approximatively 500-mg powder sample was placed in an envelope with 1 cm × 1 cm area, which is made of Al-coated Mylar tape with 50-μm thickness in order to minimize the signal from the envelope. The envelope was then attached to a low-background sample holder in a liquid-He flow-type cryostat in the temperature range between 1.8 and 250 K. At ISIS, on the other hand, a ~2 g powder sample was pressed into a disk with 23-mm diameter and 1-mm thickness and packed into an Au O-ring sealed titanium cell. The window of the cell was made of a Kapton film with 50-μm thickness. The cell was mounted onto the Al plate of a He flow-type cryofurnace in the temperature range between 50 and 500 K. The experimental techniques are described in more detail elsewhere.[54]

III. RESULTS

A. Nature of Mn^{4+} AF order at low temperature

Figure 3(a) exhibits the ZF-μ^+SR spectrum for Li_2MnO_3 obtained at the lowest T measured (1.8 K). One can clearly see the muon-spin precession signal with the frequency, $f_H \sim$ 40 MHz, demonstrating the formation of static AF order. Also, the main precession signal is found to be slightly modulated by

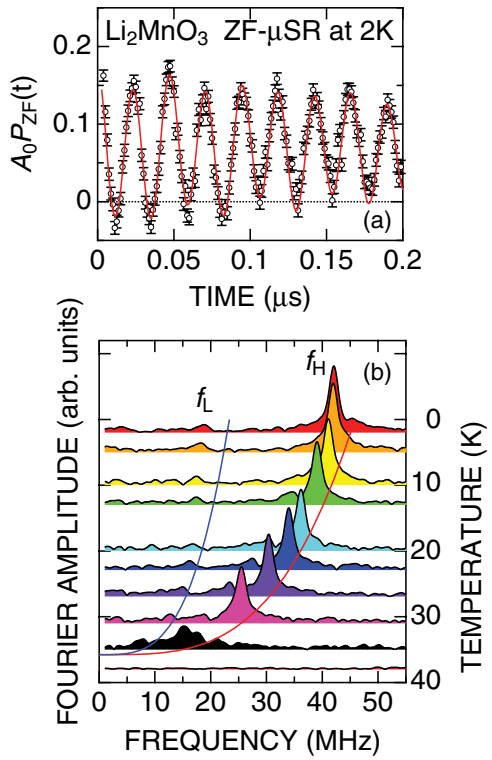

FIG. 3. (Color online) (a) The ZF-μ^+SR time spectrum for Li_2MnO_3 at 1.8 K and (b) the temperature dependence of Fourier amplitude spectrum. A solid line in (a) represents the best fit using Eq. (1). Solid lines in (b) represent a power-law fit for the $f_H(T)$ and $f_L(T)$ curves between 27 and 36 K, described in the text. These spectra were obtained at PSI.

another precession signal, which we ignored in the previous report.[42] The Fourier transform spectrum of the ZF-μ^+SR spectrum indicates that the second oscillatory signal has a frequency of ~20 MHz ($=f_L$) at 1.8 K [see Fig. 3(b)]. Since the two frequencies decrease with T and finally disappear at T_N (~35 K), the result indicates the presence of two magnetically different muon sites in the lattice.

In fact, the ZF spectra were well fitted by a combination of two exponentially relaxing cosine oscillations for the static internal field and an exponentially relaxing nonoscillatory signal:

$$A_0\,P_{ZF}(t) = A_{AF,H}\cos(2\pi f_H t + \phi_H)\exp(-\lambda_H t) + A_{AF,L}\cos(2\pi f_L t + \phi_L)\exp(-\lambda_L t) + A_{tail}\exp(-\lambda_{tail} t), \quad (1)$$

where A_0 is the initial asymmetry, $P_{ZF}(t)$ is the muon spin polarization function under ZF, $A_{AF,H}$, $A_{AF,L}$, and A_{tail} are the asymmetries associated with the three signals. $f_i(\equiv\omega_i^\mu/2\pi)$ is the muon Larmor frequency corresponding to the static internal AF field, ϕ_i is the initial phase of the oscillatory signal, λ_i and λ_{tail} are the exponential relaxation rates of the three signals.

Figure 4 shows the T dependencies of the μ^+SR parameters obtained by fitting the ZF-spectra using Eq. (1). The $f_H(T)$ and $f_L(T)$ curves exhibit an order parameter like T dependence, as expected. By using a power law, $f_i/f_i(0K) = [(T_N^{ZF} - T)/T_N^{ZF}]^\beta$, between 27 and 36 K, which corresponds to $0.25 \geqslant (T_N^{ZF} - T)/T_N$, the critical exponent (β) is estimated

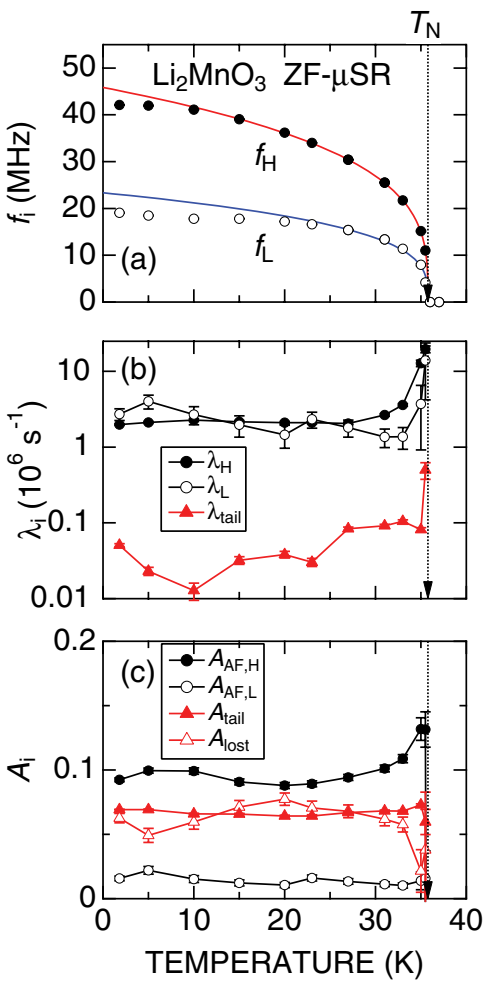

FIG. 4. (Color online) T dependencies of the μ^+SR parameters for Li_2MnO_3; (a) muon-spin precession frequencies (f_i), (b) their relaxation rates (λ_i) and the relaxation rate of nonoscillatory signal (λ_{tail}), and (c) their asymmetries (A_i and A_{tail}) and a lost asymmetry $A_{lost}(= 0.24 - A_{AF,H} - A_{AF,L} - A_{tail})$. The data were obtained by fitting the ZF spectra using Eq. (1). In (a), the solid lines on the $f_i(T)$ curve correspond to $f(T) = f(0\,K)(1 - T/T_N)^\beta$ with $f_H(0\,K) = 43.8 \pm 0.5$ MHz [$f_L(0\,K) = 23.8 \pm 0.8$ MHz], $T_N = 35.768 \pm 0.002$ K, and $\beta = 0.2916 \pm 0.0007$.

as 0.2916 ± 0.0007, $f_H(0K)$ as 43.8 ± 0.5 MHz, $f_L(0K)$ as 23.8 ± 0.8 MHz, and T_N^{ZF} as 35.768 ± 0.002 K, although we need more accurate data in the vicinity of T_N to determine β and T_N more precisely.[55,56] The obtained T_N^{ZF} is about 10 K lower than T_N (=45 K) estimated by magnetization measurements with $H \geqslant 100$ Oe [see Fig. 2(a)]. Although the reason of the discrepancy between T_N determined by magnetization and μ^+SR measurements is not clear at present, we will discuss this topic in Sec. III B. We wish, however, to point out that T_N^{ZF} is consistent with T_N determined by neutron scattering (36.5 ± 0.5 K) under zero applied field.

Although we fitted the ZF spectrum at each T using Eq. (1), $A_{AF,H}$, $A_{AF,L}$, and A_{tail} are found to be almost T independent in the T range between 1.8 and 31 K [see Fig. 4(c)]. In addition, λ_{tail} is very small compared with λ_i and roughly decreases with decreasing T [see Fig. 4(b)]. Since $A_{tail}/A_0 \sim 0.3$, the A_{tail} signal is assigned to the "1/3 tail" signal, which is

caused by the field component parallel to the initial muon-spin polarization. Here, $A_0 \sim 0.24$ was deduced from the measurements above T_N (see Sec. III B) and a reference silver sample. This also indicates the presence of a lost asymmetry (A_{lost}) in the ZF spectrum below T_N, which is simply estimated by $A_{lost} = A_0 - A_{AF,H} - A_{AF,L} - A_{tail}$. We should note that a full asymmetry was observed above T_N. Furthermore, a fast relaxing signal is unobservable in an early time domain of the ZF spectrum at 2 K [see Fig. 3(a)]. This implies the presence of a muonium state, i.e., a hydrogen-like "μ^+e^- atom," which sometimes exists in an insulator. According to the T dependence of resistivity (ρ) for Li_2MnO_3 above ~475 K,[57] ρ increases with decreasing T due to its insulating nature. Thus it is reasonable that a muonium state appears only at low T. In fact, the appearance of a muonium state only at low T is also reported for ZnO below 30 K,[58] and for GaN below 25 K.[59] Since the muonium Larmor frequency is faster by about 100 times than that of the muon, a fast relaxing signal is naturally too fast to be visible by conventional μ^+SR. The other possible explanation for A_{lost} that some muons locate at the site with a very high internal field will be discussed in Appendix.

As T increases from 2 K, the relaxation rate of the AF signals is almost T independent until ~30 K, and then increases with further increasing T towards T_N. This is a common behavior for the critical phenomenon at the AF transition. The initial phase (ϕ_i) for each oscillatory signal ranges below $\pm 20^\circ$ except in the vicinity below T_N, where its determination is difficult, suggesting commensurate AF order to the lattice. This is because a "one channel offset" of the μ^+SR spectrometer leads to a phase shift $\phi \sim 15^\circ$ for the oscillatory signal with $f = 40$ MHz. Therefore ϕ_i is assigned to be eventually zero. We will further discuss the AF spin structure for Li_2MnO_3 using the present μ^+SR result in Sec. IV B.

B. Magnetic behavior above T_N

In order to study the magnetic behavior above T_N, we also measured the μ^+SR spectrum until 70 K in a weak transverse field (wTF around 30 Oe) in a field cooling mode. Here, "weak" means that the applied field is significantly lower than any possible spontaneous internal fields (H_{int}) in the ordered state. The wTF-μ^+SR technique is sensitive to local magnetic order *via* the decrease in the amplitude (asymmetry) of the μ^+ spin precession signal and the enhanced μ^+ spin relaxation.

The wTF-μ^+SR spectrum was fitted using a combination of a slowly relaxing precessing signal due to the applied wTF and Eq. (1):

$$\begin{aligned} A_0\, P_{TF}(t) = {} & A_{TF}\cos(2\pi f_{TF}t + \phi_{TF})\exp\left(-\frac{\sigma_{TF}^2 t^2}{2}\right) \\ & + A_{AF,H}\cos(2\pi f_H t + \phi_H)\exp(-\lambda_H t) \\ & + A_{AF,L}\cos(2\pi f_L t + \phi_L)\exp(-\lambda_L t) \\ & + A_{tail}\exp(-\lambda_{tail} t), \end{aligned} \quad (2)$$

where $P_{TF}(t)$ is the muon spin polarization function under wTF, f_{TF} is the muon Larmor frequency corresponding to the applied wTF, ϕ_{TF} is the initial phase of the precessing signal, σ_{TF} is the Gaussian relaxation rate, and A_{TF} is the asymmetry

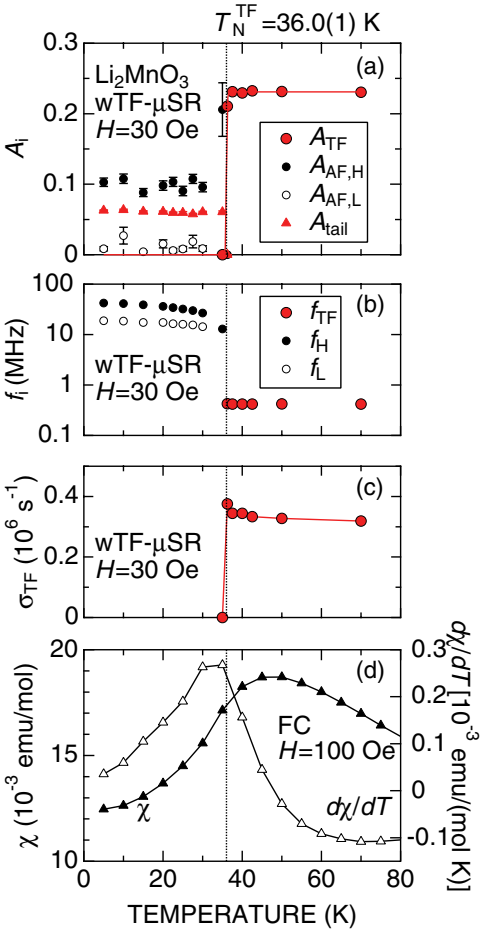

FIG. 5. (Color online) T dependencies of (a) the asymmetries (A_i), (b) the muon-spin precession frequencies (f_i), (c) Gaussian relaxation rate (σ_{TF}) for the muon-spin precession signal due to wTF, and (d) susceptibility (χ) and its slope ($d\chi/dT$) for Li_2MnO_3. Each data in (a)-(c) was obtained by fitting the wTF-spectra using Eq. (2). In (b), since wTF=30 Oe, $f_{TF} \sim 0.41$MHz. The χ data obtained with $H = 100$ Oe is the same to that in Fig. 2.

of the wTF component of the μ^+SR spectrum. Here, $A_{TF} > 0$ at $T > T_N$, but $A_{TF} = 0$ at $T \leqslant T_N$. On the contrary, $A_{AF,H} = A_{AF,L} = A_{tail} = 0$ at $T \geqslant T_N$, as seen in Fig. 4.

Figure 5 shows the T dependencies of wTF-μ^+SR parameters together with the $\chi(T)$ and $d\chi/dT(T)$ curves obtained with $H = 100$ Oe in a field cooling mode. As T decreases from 70 K, A_{TF} is almost T independent down to 37.5 K, slightly decreases at 36.5 K, and then suddenly drops to zero at 35 K. At the same T, both A_{AFh} and A_{tail} signals appear, while the A_{AFl} signal is observed at $T \leqslant 30$ K, indicating the formation of static AF order around 35 K. Below 35 K, the T dependencies of A_i and f_i are reproducible to those of A_i and f_i extracted from the ZF-μ^+SR spectra, as expected. This is because the applied wTF is negligibly small compared with the static AF field [see Fig. 5(b)].

Here, $A_{TF}(T)/A_{TF}(70\text{ K})$ corresponds to the volume fraction of paramagnetic phases in a sample. Therefore T_N^{TF} is estimated as 36.0(1) K, at which $A_{TF}(T)/A_{TF}(70\text{ K}) = 0.5$. The steplike change in the $A_{TF}(T)$ curve at T_N^{TF} and a small increase in σ_{TF} towards T_N^{TF} [see Fig. 5(c)] indicate the absence of short-range order even above the vicinity of

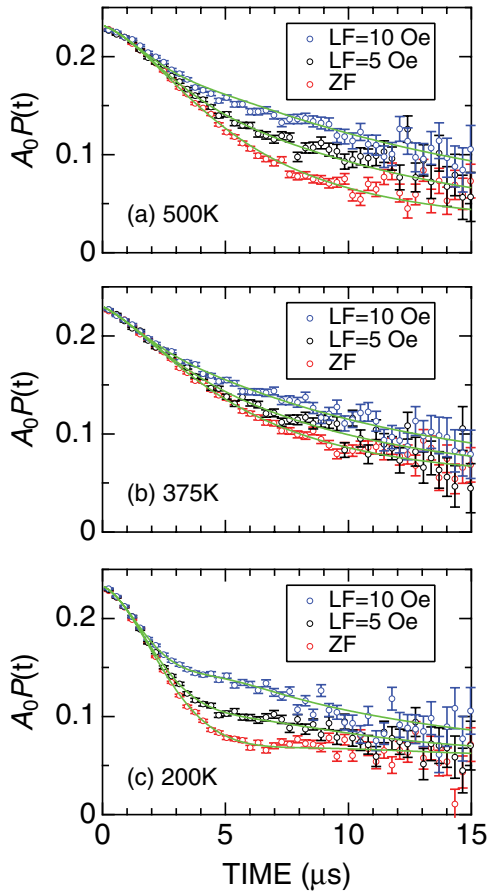

FIG. 6. (Color online) ZF- and LF-μ^+SR spectra for Li_2MnO_3 obtained at (a) 500, (b) 375, and (c) 200 K. The magnitude of LF were 5 and 10 Oe. Solid lines represent the fit result using Eq. (3). These spectra were obtained at ISIS/RAL.

T_N^{TF}. Note that T_N^{TF} is comparable to T_N obtained from the ZF measurements ($T_N^{ZF} = 35.768 \pm 0.002$ K). On the other hand, the $\chi(T)$ curve shows a broad maximum around 45 K ($=T_N^{\chi}$) even with $H = 100$ Oe. Since the $\chi(T)$ curve obtained with $H = 10$ kOe is almost identical to that obtained with $H = 100$ Oe (see Fig. 2), the discrepancy between T_N^{TF} (or T_N^{ZF}) and T_N^{χ} is an intrinsic feature for Li_2MnO_3. Interestingly, the $d\chi/dT(T)$ curve exhibits a maximum at T_N^{TF}, as in the case for a zigzag-chain compound, $CaCr_2O_4$.[60] This would suggest the effect of low dimensionality on χ in Li_2MnO_3.

C. Li^+ diffusion at high temperature

In order to know the temperature dependence of the μ^+SR spectrum in the paramagnetic state, Fig. 6 shows the ZF and LF spectrum for Li_2MnO_3 obtained at 200, 375, and 500 K. At each T, the ZF spectrum shows a damped Kubo-Toyabe behavior. This is characteristic for the case that the muon spins are depolarized by internal fields of both electronic and nuclear origin.[48] Here, the former is caused by a fluctuating magnetic field due to 3d electrons of Mn^{3+} ions (H_{int}^E), while the latter is caused by nuclear magnetic fields due to ^{6}Li, ^{7}Li, ^{55}Mn, and ^{17}O (H_{int}^N). Since the natural abundance of ^{6}Li, ^{7}Li, ^{55}Mn, and ^{17}O is 7.59%, 92.41%, 100%, and 0.038%, respectively, the effect of ^{17}O on H_{int}^N is negligibly small.

Furthermore, the applied LF (=10 or 5 Oe) clearly reduces the relaxation rate, i.e., a decoupling behavior is observed at 200 K. Although such a "decoupling" effect is very weak at 375 K, indicating the increase in a field fluctuation rate of H_{int}^N with T, the same LF decouples the relaxation rate again at 500 K. This means that H_{int}^N shows a static nature at 200 K, but dynamic at 300 K, and then becomes static again at 500 K, as in the case for olivine-type $LiMPO_4$ with M = Fe, Co, and Ni.[51,53]

In order to know the change in H_{int}^E and H_{int}^N with T, the ZF and LF spectra were fitted simultaneously by a combination of an exponentially damped dynamic Gaussian Kubo-Toyabe function [$G^{DGKT}(\Delta,\nu,t,H_{LF})$] caused by a fluctuating H_{int}^N due to ^{6}Li, ^{7}Li, and ^{55}Mn nuclear moments,[48] and an offset background (BG) signal from the fraction of muons stopped mainly in the sample cell, which is made of high-purity titanium:

$$A_0\, P_{LF}(t) = A_{KT} \exp(-\lambda t) G^{DGKT}(\Delta,\nu,t,H_{LF}) + A_{BG}, \qquad (3)$$

where A_0 is the initial ($t = 0$) asymmetry, A_{KT} and A_{BG} are the asymmetries associated with the three signals. λ is the exponential relaxation rate, Δ is the static width of the local field distribution at the disordered sites, and ν is the field fluctuation rate. When $\nu = 0$ and $H_{LF} = 0$, $G^{DGKT}(t,\Delta,\nu,H_{LF})$ is the static Gaussian KT function $G_{zz}^{KT}(t,\Delta)$ in ZF. The low-T result suggests the presence of two different muon sites in the lattice. Although such situation is expected to be the same at T above T_N, Δ for the first site is predicted to be very similar to that for the second site (see Sec. IV A). Therefore the ZF and LF spectra at high T are well fitted by Eq. (3).

At first, we fitted the ZF and LF spectra using a common A_{BG} in the whole T range and common, i.e., H_{LF} independent, Δ and ν at each T in Eq. (3). As a result, λ was found to be rather small compared with Δ and ν and almost T independent in the whole T range. Therefore we finally fitted all the ZF and LF spectra using common A_{KT}, A_{BG}, and λ. Such a global fit provided that $A_{KT} = 0.1795 \pm 0.0003$, $A_{BG} = 0.0595 \pm 0.0003$, and $\lambda = (0.0563 \pm 0.0019) \times 10^6$ s^{-1}. Here, the origin of λ is a coupling between localized Mn moments and muon-spins, where the coupling constant J_{KT} is expected to be very small, since λ is T independent.

Figure 7 shows the T dependencies of Δ, ν, and λ obtained by the global fit. As T increases from 175 K, Δ is almost

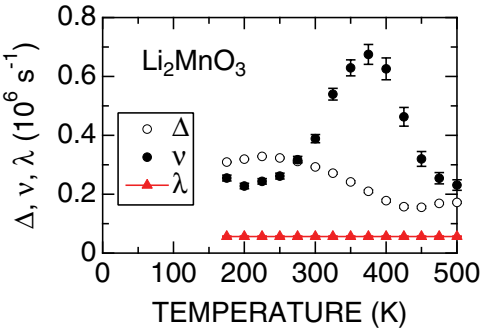

FIG. 7. (Color online) T dependencies of Δ and ν for Li_2MnO_3. The common parameter $\lambda = (0.0563 \pm 0.0019) \times 10^6$ s^{-1} is also plotted for comparison. Each set of data was obtained by global fitting the ZF and LF spectra using Eq. (3).

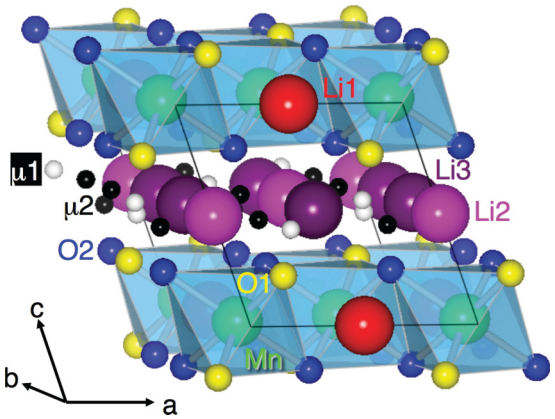

FIG. 8. (Color online) Possible muon sites ($\mu 1$ and $\mu 2$) for Li_2MnO_3 predicted by electrostatic potential calculations. Also, since there are three crystallographically different Li sites and two crystallographically different O sites in the lattice, they are represented by different colors for clarity of display. Solid lines represent a crystallographic unit cell.

independent of T until ~250 K, and decreases slightly with T, then finally levels off to a constant value ($\sim 0.16 \times 10^{-6}$ s^{-1}) above ~425 K. On the other hand, ν starts to increase above around 250 K with increasing the slope ($d\nu/dT$), reaches a maximum at 375 K and then decreases with further increasing T. Then, ν seems to level off above 475 K. Since the static behavior at high T excludes the possibility of muon-diffusion, the Li^+ ions are found to diffuse above ~300 K and their diffusion rate increases with T, as in the case for LiMPO$_4$.[51,53] When ν becomes rather large compared with Δ, such diffusion is too fast to be visible by μ^+SR, resulting in the decrease in ν with further increasing T above 375 K, and finally, ν (Δ) corresponds to the nuclear field fluctuation rate (nuclear field distribution width) mainly by immobile Li and ^{55}Mn above ~450 K. The diffusive behavior detected by μ^+SR will be discussed in detail in Sec. IV C.

IV. DISCUSSION

A. Muon sites

In the Li_2MnO_3 lattice, there are two different oxygen sites, i.e., the O1 and O2 sites, as seen in Fig. 8 and Table I. Therefore, assuming that each μ is bound to the nearest O^{2-} ion with a typical bond length for oxides, namely, $d_{\mu\text{-}O} = 1$ Å,[54] electrostatic potential (E) calculations using a point charge model suggested two possible muon sites in the vicinity of the O^{2-} ions, i.e., the $\mu 1$ and $\mu 2$ site, in the Li_2MnO_3 lattice (see Table I and Fig. 8).

The calculations also indicate that the number density of the $\mu 2$ site is twice larger than that of the $\mu 1$ site. Furthermore, E for the $\mu 2$ site is slightly lower than E for the $\mu 1$ site. Therefore the muons located at the $\mu 2$ site are most likely to provide a major signal in the μ^+SR spectrum, particularly at low T. However, in a paramagnetic state, Δ(0 K) at the $\mu 2$ site ($=0.598 \times 10^6$ s^{-1}) is very close to that at the $\mu 1$ site ($=0.562 \times 10^6$ s^{-1}). This is consistent with the fact that, at T above T_N, the ZF and LF spectra from Li_2MnO_3 were well fitted by one signal [see Eq. (3)]. Note that the dipole field calculations provide Δ at 0 K, while the lowest T, at which Δ and ν were measured, was 175 K (see Fig. 7). As a result, due to a thermally activated motion of ions and muons, the measured Δ is smaller by 40% than Δ(0K). Such discrepancy is also observed for Li_xCoO_2[29] and LiMPO$_4$[51–53] (see also Appendix).

B. AF spin structure

Here, we wish to discuss the AF spin structure, based on the present μ^+SR result. Since there are two muon sites in the Li_2MnO_3 lattice, which provide two distinct internal magnetic fields for the common AF spin structure (see Figs. 3 and 4), we have multiple viewpoints to conjecture the AF spin structure for Li_2MnO_3. This provides complimentary information to that obtained by neutron scattering, as in the case for $BaCoO_3$,[62] Ba_2CoO_4,[63] NaV_2O_4,[64,65] RCoAsO,[66] and $K_2Cr_8O_{16}$.[67]

Past neutron work reported the presence of magnetic Bragg peaks below T_N and suggested that the AF unit cell is doubled along the c axis, due to opposite moments in the adjacent $[Li_{1/3}Mn_{2/3}]O_2$ layers along the c axis. In addition, among the six possible AF models deduced from symmetry analysis, either the F_z-type or C_z-type AF order was proposed as the candidate for the AF ground state of Li_2MnO_3. Here, for the F_z-type order, the Mn moments align parallel to the c axis in the $[Li_{1/3}Mn_{2/3}]O_2$ layer but antiparallel between the adjacent $[Li_{1/3}Mn_{2/3}]O_2$ layers. On the contrary, for the C_z-type order, each Mn moment aligns parallel or antiparallel to the c axis, and an FM chain along the a axis aligns antiferromagnetically along both the b and c axis.

Table II summarizes the internal fields at the two muon sites ($H_{\mu i}$ and $f_{\mu i}$) using the six AF models estimated by dipole field calculations. Since the ordered Mn moment (μ_{Mn}^{ord}) should be less than $3\mu_B$ for Mn^{4+} with $S = 3/2$, all the F-type AF models are thought to be not suitable for Li_2MnO_3. Moreover, the ratio between the two internal fields for each F-type disagrees with the experimental result, supporting the above conclusion. On the other hand, among the three C-type AF models, either C_x or C_y is a candidate for the AF order in

TABLE I. Possible muon sites (μ_n), which locate 1 Å away from O_n, the position of the nearest O^{2-}, the position of μ_n, the distance to the nearest Mn ions ($d_{\mu\text{-Mn}}$) electrostatic potential (E) at μ_n, the number of the site per crystallographic unit cell, and the nuclear dipole field distribution width at 0 K (Δ) for Li_2MnO_3 determined by electrostatic potential calculations and dipole field calculations. The calculations were performed by a computer program DIPELEC,[61] which uses a point charge model.

Site	Nearest O site (x,y,z)	(x,y,z)	$d_{\mu\text{-Mn}}$(Å)	E (eV)	Number/unit cell	$\Delta(10^6)$s^{-1}
$\mu 1$	O1 (0.2189,0.0000,0.2273)	(0.3213,0.0000,0.4355)	2.6441	−10.558	4	0.598
$\mu 2$	O2 (0.2540,0.3211,0.2233)	(0.2974,0.3452,0.4278)	2.6518	−10.624	8	0.562

TABLE II. The internal magnetic field at the two muon sites for the six AF models proposed by neutron. The AF model C_n and F_n with $n = x,y,z$, the internal magnetic field (H) at the $\mu1$ and $\mu2$ site, the maximum value of the muon-spin precession frequency ($f_{\mu i}^{\max}$) at the $\mu1$ and $\mu2$ site, the ratio between the two $f_{\mu i}^{\max}$s, and the ordered Mn moment ($\mu_{\mathrm{Mn}}^{\mathrm{ord}}$). Note that the AF unit cell is twice as large along the c axis. The F_n order corresponds to the A-type AF order along the c axis, namely, the Mn moments align ferromagnetically in the $[Li_{1/3}Mn_{2/3}]O_2$ layer but antiferromagnetically between the adjacent $[Li_{1/3}Mn_{2/3}]O_2$ layers. For the F_x (F_y, F_z) order, the Mn moments align parallel or antiparallel to the a (b, c) axis. On the other hand, for the C_x (C_y, C_z) order, each Mn moment aligns parallel or antiparallel to the a (b, c) axis, and an FM chain along the a axis aligns antiferromagnetically along both the b and c axis. $f_{\mu i}^{\max}$ is $f_{\mu i}$ when $\mu_{\mathrm{Mn}}^{\mathrm{ord}}$ is the theoretical value of Mn^{4+} with $S = 3/2$ ($3\ \mu_{\mathrm{B}}$).

AF order	$H_{\mu1}$(Oe/μ_{B})	$H_{\mu2}$(Oe/μ_{B})	$f_{\mu1}^{\max}$(MHz)	$f_{\mu2}^{\max}$(MHz)	$f_{\mu1}/f_{\mu2}$	$\mu_{\mathrm{Mn}}^{\mathrm{ord}}(\mu_{\mathrm{B}})$
F_x	645	598	26.2	24.3	1.078	4.82
F_y	207	601	8.4	24.4	0.345	5.18
F_z	548	873	22.3	35.5	0.628	3.56
C_x	566	1187	23.0	48.3	0.476	2.62
C_y	1040	495	42.3	20.1	2.104	2.99
C_z	873	1110	35.5	45.1	0.787	2.80
experiment			19.09 ± 0.05	42.14 ± 0.06	0.453	

Li_2MnO_3. Here, we should remind that the muons at the $\mu2$ site provide a major signal, leading to $H_{\mu2} > H_{\mu1}$. Therefore the most probable AF order for Li_2MnO_3 is determined as the C_x-type order, as shown in Fig. 9. The C_x-type order is reasonably formed when the interaction between the nearest neighboring Mn ions is AF and the interaction via the Mn-O-Li-O-Mn path is AF both along the c axis and in the ab plane. Indeed, $\mu_{\mathrm{Mn}}^{\mathrm{ord}}$ is estimated as $2.62\mu_{\mathrm{B}}$ at 1.8 K, which is in good agreement with the neutron result ($2.7 \pm 0.3\mu_{\mathrm{B}}$) at 4 K.

According to the simulation of the neutron diffraction patterns with the wavelength $\lambda_{\mathrm{n}} = 2.522$ Å, the F_z-type order yields a magnetic diffraction peak at $2\theta = 15.1^\circ$ with the intensity of 75% of that at $2\theta = 34.1^\circ$. The peak at $2\theta = 15.1^\circ$ is the most intense magnetic diffraction peak for both the F_x and F_y-type order. On the other hand, such diffraction peak no longer exists for the C-type order. Moreover, either C_x or C_z-type order provides an acceptable result for explaining the reported diffraction pattern. Therefore the F-type order is highly unlikely to fit the experimental data, but either the C_x- or C_z-type order is more likely. Consequently, the C_x-type AF order is very reasonable both for the present μ^+SR result and past neutron data.

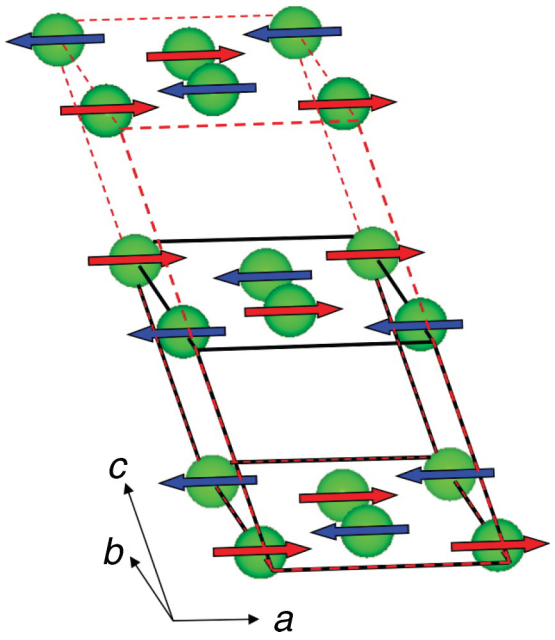

FIG. 9. (Color online) The C_x-type AF spin structure for Li_2MnO_3 proposed by the present μ^+SR investigation. Red and blue arrows correspond to the Mn moment. Note that only Mn ions are shown for clarity of display. Solid lines represent a crystallographic unit cell, while broken lines represent a magnetic unit cell.

Furthermore, we consider the effect of the FM arrangement in the F-type order on H_μ, namely, the hyperfine field (H_{hf}) due to the local spin density at the muon site might significantly contribute to H_μ, as in the case of ferromagnetic RCoAsO and $K_2Cr_8O_{16}$.[66,67] For the compound with an α-$NaFeO_2$-type structure, F-type AF order is known to be formed in $NaNiO_2$ below $T_{\mathrm{N}} \sim 23$ K.[24,68] However, the observed H_μ($\sim$60 MHz at 2 K) was in good agreement with the prediction from dipole field calculations.[40] This suggests that H_{hf} is not so large compared with that for ferromagnetic materials. Hence it is reasonable that the F-type order is excluded for Li_2MnO_3, based on the comparison between the measured H_μ and the prediction from dipole field calculations.

C. Li diffusive behavior

We attempt to evaluate a self-diffusion coefficient of Li^+ ions (D_{Li}) using the present μ^+SR result. At first, we need to determine the diffusion pathway(s) of Li^+. Here, we should note that there are three different Li sites in the lattice (see Fig. 8). Also, since the regular Li1 site is fully occupied by Li, we naturally consider only the jump to interstitial sites. The electrostatic potential calculations suggest six possible interstitial sites for the Li2 and Li3 sites in the ab plane, whereas two possible interstitial sites for the Li1 and Li3 site in the bc plane (see Fig. 10).

Then, we focus on the decrease in Δ due to Li diffusion. That is, when Li^+ ions diffuse too fast, i.e., $\nu \gg \Delta$, such diffusion is invisible by μ^+SR. As a result, Δ gradually decreases with T above 250 K, and finally, Δ approaches to the Δ ($\sim 0.18 \times 10^6$ s^{-1}) caused by immobile Li and ^{55}Mn. In

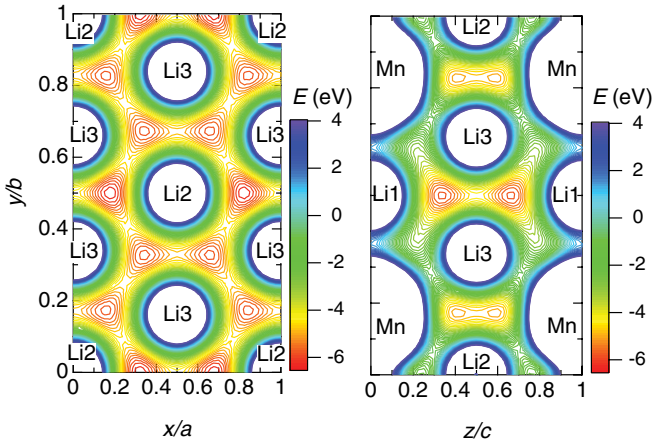

FIG. 10. (Color online) Electrostatic potential distribution in (a) the $(x,y,0.5)$ plane and (b) the $(0,y,z)$ plane for Li_2MnO_3. The lattice constants are $a = 4.937$Å, $b = 8.532$Å, $c = 5.030$Å, and $\beta = 109.46°$.

other words, we could deduce the mobile Li^+ from the change in Δ. Thus the magnitude of Δ was estimated for the Li_xMnO_3 phase without Li1, Li2, and/or Li3 by dipole field calculations (see Table III). Comparing with the experimental result at 200 and 500 K, it is clearly excluded that the Li^+ ions at the Li2 and Li3 sites, i.e., all the Li^+ ions in the Li plane, become mobile at high T, because $\Delta_{\mu i}(-\text{Li2},-\text{Li3})$ are too small for explaining the experimental result. Also, it is most unlikely that only the Li^+ ions at the Li2 site are mobile at high T.

Therefore the most reasonable scenario is that the Li^+ ions at the Li3 and Li1 sites are mobile at high T, but the Li^+ ions at the Li2 site are still immobile even at 500 K. In other words, the Li^+ ions are diffusing not in the Li plane, i.e., in the ab plane, but along the c axis through the Li^+ ions in the $[Li_{1/3}Mn_{2/3}]$ plane (Li1 site). This is consistent with the prediction from first-principles calculations[69] in which Li_xMnO_3 with Li vacancies in both the Li and $[Li_{1/3}Mn_{2/3}]$ planes is more stable than that with Li vacancies only in the Li plane. Thus we will consider the two diffusion pathways in the bc plane [see Fig. 10(b)]; namely, one is the pathway from the Li1 site to the interstitial site at (0.0019,0.5000,0.3374) along the c axis, and the other is the pathway from the Li3 site to the same interstitial site.

Assuming that ν corresponds to the jump rate of the Li^+ ions between the neighboring sites, D_{Li} is given by[70]

$$D_{\text{Li}} = \sum_{i=1}^{n} \frac{1}{N_i} Z_{v,i} s_i^2 \nu, \tag{4}$$

where N_i is the number of Li sites in the ith path, $Z_{v,i}$ is the vacancy fraction, and s_i is the jump distance. Based on the above consideration, $n = 2$, $N_1 = 2$, and $Z_1 = 1$ and $N_2 = 2$, and $Z_2 = 1$. From Fig. 10, $s_1 = 1.697$Å and $s_2 = 1.596$Å. In order to extract ν due to Li diffusion, we fitted the ν-versus-$1/T$ curve by a combination of a thermal activation process due to Li diffusion and a T-independent offset signal caused by the fluctuation of Mn moments [see Fig. 11(a)]. That is, $\nu = \nu_0 \exp(-E_a/k_B T) + \nu_{\text{Mn}}$, where E_a is the activation energy and k_B is the Boltzmann's constant. Such fit provides that $\nu_0 = (75.577 \pm 0.001) \times 10^6 \text{s}^{-1}$, $E_a = 0.156 \pm 0.003$ eV, and $\nu_{\text{Mn}} = (0.22 \pm 0.05) \times 10^6 \text{s}^{-1}$. Using $(\nu - \nu_{\text{Mn}})$ instead of ν in Eq. (4), we have obtained the T dependence of D_{Li} for Li_2MnO_3 [see Fig. 11(b)]. However, there are, to our knowledge, no available data on D_{Li} from neither other experiments, nor calculations.

Concerning E_a, the value obtained by μ^+SR is about 1/3 of E_a (0.45eV) estimated from ac impedance measurements for a powder sample.[46] The discrepancy between E_a obtained by μ^+SR and ac impedance is due to the fact that μ^+SR is specially sensitive to a short-range jump of Li^+ ions, while ac impedance senses the long-range Li diffusion. In other words, since μ^+SR is a local probe, a powder sample is approximately equivalent to a single-crystal sample for muons. A very similar discrepancy between E_a obtained by NMR and ac impedance is also reported for several materials.[71]

Finally, we wish to point out the diffusive nature of the Li-overstiochiometric $LiMO_2$ compounds, such as, $Li_{1+\delta}Co_{1-\delta}O_{2-\delta}$[72] and $Li_{1+\delta}(Co_{0.333}Ni_{0.333}Mn_{0.333})_{1-\delta}O_2$.[23] For these compounds, the excess Li^+ ions naturally locate at the M site in the MO_2 layers. Based on the present result, such Li^+ ions are likely to make an additional pathway of Li diffusion along the c axis. In order to know the effect of δ on

TABLE III. The predicted variation of the field distribution width at 0 K (Δ) with the vacant Li sites. Here, we assume that, when the Li^+ ions diffuse too fast to be visible by μ^+SR, Δ decreases as if such Li ions are absent in the lattice. The experimental results obtained at 200 and 500 K are also listed for comparison. Here, since the muons at the $\mu 2$ site are expected to contribute to the major signal, $\Delta_{\mu 2}$ and $\Delta_{\mu 2}/\Delta_{\mu 2}^{\text{none}}$ should be compared with the experimental result.

Vacant Li	$\Delta_{\mu 1}(10^6\ \text{s}^{-1})$	$\Delta_{\mu 2}(10^6\ \text{s}^{-1})$	$\Delta_{\mu 1}/\Delta_{\mu 1}^{\text{none}}$	$\Delta_{\mu 2}/\Delta_{\mu 2}^{\text{none}}$
none	0.598	0.562	1	1
Li1	0.587	0.552	0.981	0.983
Li2	0.526	0.449	0.879	0.799
Li3	0.336	0.383	0.562	0.682
Li2 and Li3	0.178	0.180	0.298	0.321
Li3 and Li1	0.315	0.369	0.527	0.656
Li1 and Li2	0.513	0.437	0.858	0.778
Li1, L2, and Li3	0.135	0.148	0.226	0.264
experiment	Δ(200 K) ($10^6\ \text{s}^{-1}$)	Δ(500 K) ($10^6\ \text{s}^{-1}$)	Δ(500 K)/Δ(200 K)	
	0.3411 ± 0.0013	0.1725 ± 0.0034	0.506	

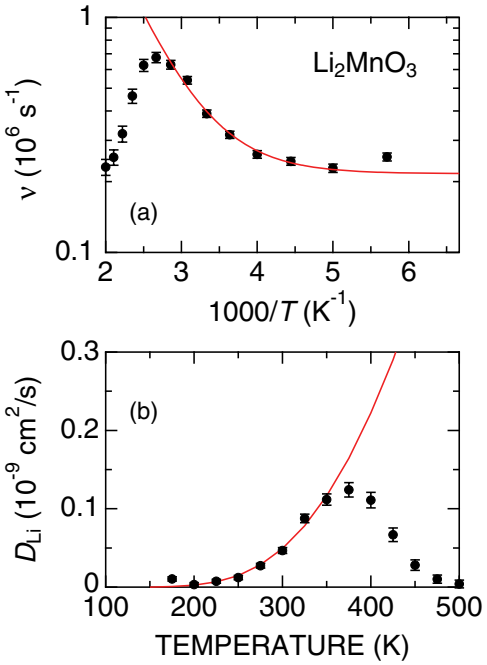

FIG. 11. (Color online) (a) The relationship between ν and $1/T$ and (b) the T dependence of D_{Li} for Li_2MnO_3. In (a), a solid line shows a combination of a thermal activation process and a T independent offset discussed in the text. In (b), a solid line shows the predicted $D_{\mathrm{Li}}(T)$ curve from the thermal activation process.

the diffusive nature, it would be very interesting to measure D_{Li} as a function of δ.

V. SUMMARY

We have investigated the low-T magnetic nature and high-T diffusive behavior of Li_2MnO_3 using a unique local magnetic probe, i.e., the muon-spin rotation and relaxation (μ^+SR) technique. Detailed analysis plus dipole field calculations suggested the formation of the C_x-type AF order below $T_{\mathrm{N}} = 35.768 \pm 0.002$ K, contrary to the F_z-type order proposed by past neutron measurements. From the temperature dependence of a nuclear field relaxation in a paramagnetic state, Li^+ ions were found to start diffusing above 200 K. Based on the temperature dependence of the field distribution width, the diffusion pathway was assigned along the c axis. Using this diffusion pathway and the field fluctuation rate, a self-diffusion coefficient of Li^+ ions was estimated as $(4.7 \pm 0.4) \times 10^{-11}$ cm^2/s at 300 K.

ACKNOWLEDGMENTS

We thank the staff of PSI and ISIS for help with the μ^+SR experiments. D.A. acknowledges financial support from the Romanian UEFISCDI Project No.PN-II-ID-PCE-2011-3-0583 (85/2011). This work was also supported by the "UltraSlow Muon Microscope" (No. 23108003) Grant-in Aid for Scientific Research on Innovative Areas from the Ministry of Education, Culture, Sports, Science and Technology (MEXT) of Japan. All images involving crystal structure were made with VESTA.[73]

APPENDIX: EFFECT OF μ-O DISTANCE ON CALCULATED RESULTS

Here, we wish to show the reliability of the assumption that each μ is bound to the nearest O^{2-} ion with the distance, $d_{\mu\text{-O}} = 1$ Å. Figure 12 shows the $d_{\mu\text{-O}}$ dependencies of $\Delta_{\mu i}$, $E_{\mu i}$, $f_{\mu i}$ for the F_n order, and $f_{\mu i}$ for the C_n order. As $d_{\mu\text{-O}}$ increases, the distance between μ^+ and the nearest Li decreases, while that between μ^+ and the nearest Mn increases. As a result, the change in $\Delta_{\mu i}$ is about 10%, even when $d_{\mu\text{-O}}$ varies from 0.8 to 1.2 Å. Also, $E_{\mu 1}$ is very close to $E_{\mu 2}$ in the whole calculated range, while $E_{\mu 1} > E_{\mu 2}$ when $d_{\mu\text{-O}} \leqslant 1.0$Å, and $E_{\mu 1} < E_{\mu 2}$ when $d_{\mu\text{-O}} > 1.0$ Å.

For the F_n order, there is no combination of $f_{\mu 1}$ and $f_{\mu 2}$ to satisfy the two precession frequencies, f_{H} and f_{L}, in the $d_{\mu\text{-O}}$ range between 0.8 and 1.2 Å. On the other hand, for the C_n order, both the C_x and C_y orders agree with the experimental result. Since $f_{\mu i}$ is calculated for $\mu^{\mathrm{ord}}_{\mathrm{Mn}} = 3\mu_{\mathrm{B}}$, it is also found

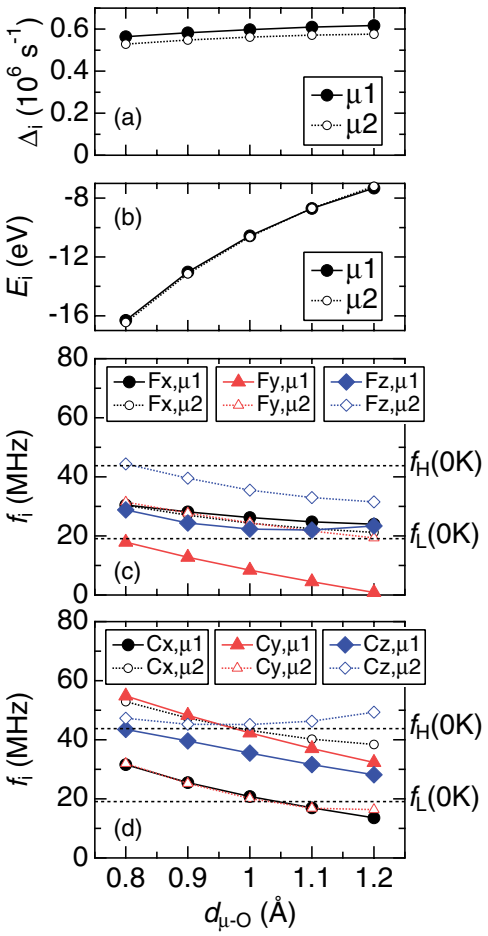

FIG. 12. (Color online) The $d_{\mu\text{-O}}$ dependencies of (a) $\Delta_{\mu i}$, (b) $E_{\mu i}$, (c) $f_{\mu i}$ for the F_n order, and (d) $f_{\mu i}$ for the C_n order. In (c) and (d), $\mu^{\mathrm{ord}}_{\mathrm{Mn}} = 3\mu_{\mathrm{B}}$.

that $d_{\mu\text{-O}} \leqslant 1$Å. Considering $E_{\mu i}$ and the number of the $\mu 1$ and $\mu 2$ sites in the unit cell, the C_x order is more likely for the AF spin structure than the C_y order.

Figure 12 also indicates that the highest internal field at the muon site is $H_\mu = 55$ MHz (=4.06 kOe) for the C_y order with $d_{\mu\text{-O}} = 0.8$ Å or $H_\mu = 53$ MHz (=3.91 kOe) for the C_x order with $d_{\mu\text{-O}} = 0.8$ Å. This means that all the signals from the muons in the Li_2MnO_3 lattice of the AF-ordered phase range in the time window of μ^+SR. Therefore A_{lost} below T_N is most unlikely to be caused by the muons located at the site with very high H_μ, but highly likely to be caused by the muonium formation.

*e0589@mosk.tytlabs.co.jp

[1] P. W. Anderson, Mat. Res. Bull. **8**, 153 (1973).
[2] K. Hirakawa, H. Kadowaki, and K. Ubukoshi, J. Phys. Soc. Jpn. **54**, 3526 (1985).
[3] H. R. Krishnamurthy, C. Jayaprakash, S. Sarker, and W. Wenzel, Phys. Rev. Lett. **64**, 950 (1990).
[4] K. Mizushima, P. C. Jones, P. J. Wiseman, and J. B. Goodenough, Mat. Res. Bull. **15**, 783 (1980).
[5] M. G. S. R. Thomas, W. I. F. David, and J. B. Goodenough, Mat. Res. Bull. **10**, 1137 (1985).
[6] M. S. Whittingham, Chem. Rev. **104**, 4271 (2004).
[7] V. Pralong, Prog. Solid State Chem. **37**, 262 (2009).
[8] P. Strobel and B. Lambert-Andron, J. Solid State Chem. **75**, 90 (1988).
[9] V. M. Jansen and R. Hoppe, Z. Anorg. Allg. Chem. **397**, 279 (1973).
[10] V. G. Meyer and R. Hoppe, Z. Anorg. Allg. Chem. **424**, 257 (1976).
[11] M. H. Rossouw and M. M. Thackeray, Mat. Res. Bull. **26**, 467 (1991).
[12] Y. Shao-Horn, Y. Ein-ElI, A. D. Robertson, W. F. AveriII, S. A. Hackney, and J. W. F. Howard, J. Electrochem. Soc. **145**, 16 (1998).
[13] P. Kalyani, S. Chitra, T. Mohan, and S. Gopukumar, J. Power Sources **80**, 103 (1999).
[14] C. Johnson, S. Korte, J. Vaughey, M. M. Thackeray, T. Bofinger, Y. Shao-Horn, and S. Hackney, J. Power Sources **81–82**, 491 (1999).
[15] S.-H. Park, Y. Sato, J.-K. Kim, and Y.-S. Lee, Mater. Chem. Phys. **102**, 225 (2007).
[16] C. H. Lei, J. G. Wen, M. Sardela, J. Bareno, I. Petrov, S.-H. Kang, and D. P. Abraham, J. Mater. Sci. **44**, 5579 (2009).
[17] D. Y. W. Yu, K. Yanagida, Y. Kato, and H. Nakamura, J. Electrochem. Soc. **156**, A417 (2009).
[18] A. Boulineau, L. Croguennec, C. Delmas, and F. Weill, Solid State Ionics **180**, 1652 (2010).
[19] Z. Lu and J. R. Dahn, J. Electrochem. Soc. **149**, A815 (2002).
[20] A. D. Robertson and P. G. Bruce, Chem. Mater. **15**, 1984 (2003).
[21] Y. Okamoto, J. Electrochem. Soc. **159**, A152 (2012).
[22] D. Y. W. Yu and K. Yanagida, J. Electrochem. Soc. **158**, A1015 (2011).
[23] M. M. Thackeray, S.-H. Kang, C. S. Johnson, J. T. Vaughey, R. Benedeka, and S. A. Hackney, J. Mater. Chem. **17**, 3112 (2007).
[24] M. J. Lewis, B. D. Gaulin, L. Filion, C. Kallin, A. J. Berlinsky, H. A. Dabkowska, Y. Qiu, and J. R. D. Copley, Phys. Rev. B **72**, 014408 (2005).
[25] J. Sugiyama, M. Månsson, Y. Ikedo, T. Goko, K. Mukai, D. Andreica, A. Amato, K. Ariyoshi, and T. Ohzuku, Phys. Rev. B **79**, 184411 (2009).
[26] A. Olariu, P. Mendels, F. Bert, L. K. Alexander, A. V. Mahajan, A. D. Hillier, and A. Amato, Phys. Rev. B **79**, 224401 (2009).
[27] A. Olariu, P. Mendels, F. Bert, B. G. Ueland, P. Schiffer, R. F. Berger, and R. J. Cava, Phys. Rev. Lett. **97**, 167203 (2006).
[28] J. Sugiyama, H. Nozaki, J. H. Brewer, E. J. Ansaldo, G. D. Morris, and C. Delmas, Phys. Rev. B **72**, 144424 (2005).
[29] K. Mukai, Y. Ikedo, H. Nozaki, J. Sugiyama, K. Nishiyama, D. Andreica, A. Amato, P. L. Russo, E. J. Ansaldo, J. H. Brewer *et al.*, Phys. Rev. Lett. **99**, 087601 (2007).
[30] J. Sugiyama, H. Itahara, J. H. Brewer, E. J. Ansaldo, T. Motohashi, M. Karppinen, and H. Yamauchi, Phys. Rev. B **67**, 214420 (2003).
[31] J. Sugiyama, J. H. Brewer, E. J. Ansaldo, H. Itahara, T. Tani, M. Mikami, Y. Mori, T. Sasaki, S. Hébert, and A. Maignan, Phys. Rev. Lett. **92**, 017602 (2004).
[32] J. Sugiyama, J. H. Brewer, E. J. Ansaldo, B. Hitti, M. Mikami, Y. Mori, and T. Sasaki, Phys. Rev. B **69**, 214423 (2004).
[33] S. P. Bayrakci, C. Bernhard, D. P. Chen, B. Keimer, R. K. Kremer, P. Lemmens, C. T. Lin, C. Niedermayer, and J. Strempfer, Phys. Rev. B **69**, 100410 (2004).
[34] P. Mendels, D. Bono, J. Bobroff, G. Collin, D. Colson, N. Blanchard, H. Alloul, I. Mukhamedshin, F. Bert, A. Amato *et al.*, Phys. Rev. Lett. **94**, 136403 (2005).
[35] G. Lang, J. Bobroff, H. Alloul, P. Mendels, N. Blanchard, and G. Collin, Phys. Rev. B **72**, 094404 (2005).
[36] J. Sugiyama, H. Nozaki, Y. Ikedo, K. Mukai, J. H. Brewer, E. J. Ansaldo, G. D. Morris, D. Andreica, A. Amato, T. Fujii *et al.*, Phys. Rev. Lett. **96**, 037206 (2006).
[37] J. Sugiyama, Y. Ikedo, P. L. Russo, H. Nozaki, K. Mukai, D. Andreica, A. Amato, M. Blangero, and C. Delmas, Phys. Rev. B **76**, 104412 (2007).
[38] J. Sugiyama, K. Mukai, Y. Ikedo, P. L. Russo, H. Nozaki, D. Andreica, A. Amato, K. Ariyoshi, and T. Ohzuku, Phys. Rev. B **78**, 144412 (2008).
[39] J. Sugiyama, Y. Ikedo, K. Mukai, H. Nozaki, M. Månsson, O. Ofer, M. Harada, K. Kamazawa, Y. Miyake, J. H. Brewer *et al.*, Phys. Rev. B **82**, 224412 (2010).
[40] P. J. Baker, T. Lancaster, S. J. Blundell, M. L. Brooks, W. Hayes, D. Prabhakaran, and F. L. Pratt, Phys. Rev. B **72**, 104414 (2005).
[41] J. Sugiyama, Y. Ikedo, O. Ofer, M. Månsson, E. J. Ansaldo, J. H. Brewer, K. H. Chow, H. Sakurai, and E. Takayama-Muromachi, J. Phys. Soc. Jpn. **78**, 084715 (2009).
[42] K. Mukai, J. Sugiyama, Y. Ikedo, H. Nozaki, K. Kamazawa, D. Andreica, A. Amato, M. Månsson, J. H. Brewer, E. J. Ansaldo *et al.*, J. Phys. Chem. C **114**, 11320 (2010).
[43] I. Tomeno and M. Oguchi, J. Phys. Soc. Jpn. **67**, 318 (1998).
[44] K. Nakamura, M. Yamamoto, K. Okamura, Y. Michihiro, I. Nakabayashi, and T. Kanashiro, Solid State Ionics **121**, 301 (1999).
[45] P. Mustarelli, V. Massarotti, M. Bini, and D. Capsoni, Phys. Rev. B **55**, 12018 (1997).
[46] K. Nakamura, H. Hirano, Y. Michihiro, and T. Moriga, Solid State Ionics **181**, 1359 (2010).

[47]J. Sugiyama, K. Mukai, Y. Ikedo, H. Nozaki, M. Månsson, and I. Watanabe, Phys. Rev. Lett. **103**, 147601 (2009).
[48]T. Matsuzaki, K. Nishiyama, K. Nagamine, T. Yamazaki, M. Senba, J. M. Bailey, and J. H. Brewer, Phys. Lett. A **123**, 91 (1989).
[49]R. S. Hayano, Y. J. Uemura, J. Imazato, N. Nishida, T. Yamazaki, and R. Kubo, Phys. Rev. B **20**, 850 (1979).
[50]J. Sugiyama, ISIS experimental report No. 1120132.
[51]J. Sugiyama, H. Nozaki, M. Harada, K. Kamazawa, O. Ofer, M. Månsson, J. H. Brewer, E. J. Ansaldo, K. H. Chow, Y. Ikedo *et al.*, Phys. Rev. B **84**, 054430 (2011).
[52]P. J. Baker, I. Franke, F. L. Pratt, T. Lancaster, D. Prabhakaran, W. Hayes, and S. J. Blundell, Phys. Rev. B **84**, 174403 (2011).
[53]J. Sugiyama, H. Nozaki, M. Harada, K. Kamazawa, Y. Ikedo, Y. Miyake, O. Ofer, M. Månsson, E. J. Ansaldo, K. H. Chow *et al.*, Phys. Rev. B **85**, 054111 (2012).
[54]G. M. Kalvius, D. R. Noakes, and O. Hartmann, *Handbook on the Physics and Chemistry of Rare Earths* (North-Holland, Amsterdam, 2001), Vol. 32, Chap. 206, pp. 55–451.
[55]W. B. Yelon, D. E. Cox, and M. Eibschütz, Phys. Rev. B **12**, 5007 (1975).
[56]A. Taroni, S. T. Bramwell, and P. C. W. Holdsworth, J. Phys.: Condens. Matter **20**, 275233 (2008).
[57]V. Massarotti, D. Capsoni, M. Bini, G. Chiodelli, C. B. Azzoni, M. C. Mozzati, and A. Paleari, J. Solid State Chem. **131**, 94 (1997).
[58]K. Shimomura, K. Nishiyama, and R. Kadono, Phys. Rev. Lett. **89**, 255505 (2002).
[59]K. Shimomura, R. Kadono, K. Ohishi, M. Mizuta, M. Saito, K. H. Chow, B. Hitti, and R. L. Lichti, Phys. Rev. Lett. **92**, 135505 (2004).
[60]F. Damay, C. Martin, V. Hardy, A. Maignan, G. André, K. Knight, S. R. Giblin, and L. C. Chapon, Phys. Rev. B **81**, 214405 (2010).
[61]K. M. Kojima, J. Yamanobe, H. Eisaki, S. Uchida, Y. Fudamoto, I. M. Gat, M. I. Larkin, A. Savici, Y. J. Uemura, P. P. Kyriakou *et al.*, Phys. Rev. B **70**, 094402 (2004).
[62]H. Nozaki, M. Janoschek, B. Roessli, J. Sugiyama, L. Keller, J. H. Brewer, E. J. Ansaldo, G. D. Morris, T. Takami, and H. Ikuta, Phys. Rev. B **76**, 014402 (2007).
[63]P. L. Russo, J. Sugiyama, J. H. Brewer, E. J. Ansaldo, S. L. Stubbs, K. H. Chow, R. Jin, H. Sha, and J. Zhang, Phys. Rev. B **80**, 104421 (2009).
[64]J. Sugiyama, Y. Ikedo, T. Goko, E. J. Ansaldo, J. H. Brewer, P. L. Russo, K. H. Chow, and H. Sakurai, Phys. Rev. B **78**, 224406 (2008).
[65]O. Ofer, Y. Ikedo, T. Goko, M. Månsson, J. Sugiyama, E. J. Ansaldo, J. H. Brewer, K. H. Chow, and H. Sakurai, Phys. Rev. B **82**, 094410 (2010).
[66]J. Sugiyama, M. Månsson, O. Ofer, K. Kamazawa, M. Harada, D. Andreica, A. Amato, J. H. Brewer, E. J. Ansaldo, H. Ohta *et al.*, Phys. Rev. B **84**, 184421 (2011).
[67]J. Sugiyama, H. Nozaki, M. Månsson, K. Prša, D. Andreica, A. Amato, M. Isobe, and Y. Ueda, Phys. Rev. B **85**, 214407 (2012).
[68]C. Darie, P. Bordet, S. de Brion, M. Holzapfel, O. Isnard, A. Lecchi, J. E. Lorenzo, and E. Suard, Eur. Phys. J. B **43**, 159 (2005).
[69]Y. Koyama, I. Tanaka, M. Nagao, and R. Kanno, J. Power Sources **189**, 798 (2009).
[70]R. J. Borg and G. J. Dienes, *An Introduction to Solid State Diffusion* (Academic Press, San Diego, 1988), Chap. 3, pp. 53–77.
[71]P. Heitjans and S. Indris, J. Phys.: Condens. Matter **15**, R1257 (2003).
[72]S. Levasseur, M. Ménétrier, Y. Shao-Horn, L. Gautier, A. Audemer, G. Demazeau, A. Largeteau, and C. Delmas, Chem. Mater. **15**, 348 (2003).
[73]K. Momma and F. Izumi, J. Appl. Cryst. **41**, 653 (2008).